

# Augmented Equivariant Attention Networks for Electron Microscopy Image Super-Resolution

Yaochen Xie, Yu Ding, Shuiwang Ji, *Senior Member, IEEE*,

**Abstract**—Taking electron microscopy (EM) images in high-resolution is time-consuming and expensive and could be invasive to samples. Advances in deep learning enable us to perform super-resolution computationally, so as to obtain high-resolution images from low-resolution ones. When training super-resolution models on pairs of experimentally acquired EM images, prior models suffer from performance loss while using the pooled-training strategy due to their inability to capture inter-image dependencies and common features shared among images. Although there exist methods that take advantage of shared features among input instances in image classification tasks, they cannot be applied to super-resolution tasks because they fail to preserve the equivariance property to spatial permutations, which is an essential property in image-to-image transformation problems. To address these limitations, we propose the augmented equivariant attention networks (AEANets) with better capability to capture inter-image dependencies and shared features, while preserving the equivariance property. The proposed AEANets captures inter-image dependencies and common features shared among images via two augmentations on the attention mechanism; namely, the shared references and the batch-aware attention during training. We theoretically show the equivariance property of the proposed augmented attention model and experimentally show that AEANets consistently outperforms the baselines in both quantitative and visual results.

**Index Terms**—Attention networks, equivariance, electron microscopy, super-resolution

## 1 INTRODUCTION

Image super-resolution started with the multiframe super-resolution approach more than 35 years ago [1] and shifted its focus to single-image super-resolution at the turn of the century [2], [3]. The latest trend is the use and development of deep-learning approaches for image super-resolution [4], [5], [6], [7].

Deep learning approaches consider the super-resolution as an image-to-image transformation task, in the sense that pairs of images, of the same size but different resolutions, are used to train the deep neural networks. A common approach to construct the training image pairs is to take a high-resolution (HR) image, acquired directly by a physical imaging device, and then synthesize the low-resolution (LR) counterpart by blurring and downsampling the high-resolution image. Datasets constructed via such an approach are called the synthetic datasets, which are rather popular and widely used in the research and practice for image super-resolution.

Very recently, [8] discussed a different type of image super-resolution problem, which involves paired HR and LR images for training, both physically acquired through the use of electron microscopes (EM). This type of images are obtained in material research for material characterization

purpose. The same material is imaged by the same electron microscope twice, each time with a different magnification, thereby producing images in two different resolutions (multi-level magnifications producing multi-resolution images is also physically possible). The HR image covers a subset of the viewfield of the LR image. When the magnification ratio is 2:1, the HR image covers 25% of the area covered by the LR image but with the same amount of pixels. Effectively, for that 25% area, the HR image entertains an image resolution doubling that of the LR image. Two such examples are shown in [8] as their Figure 1.

*Qian et al.* [8] noted a few uniqueness in the case of paired EM material images: (a) The physics behind the EM images is different from that of the natural light images, due to different imaging devices involved. Electron microscopes use electrons for imaging, which are far heavier than photons in natural light, whose static mass is zero. (b) The material images embody different image features from the daily life photos. For instance, material images have far fewer straight lines and far more wiggly and zigzagging boundaries. (c) The EM image pairs are both physically acquired. (d) The paired images are strongly connected via the subset of the viewfield where the HR and LR images overlap. *Qian et al.* [8] opined that considering the uniqueness noted above, training a deep learning model using synthetic datasets is no longer a good strategy. Their preliminary analysis demonstrated that doing so can lead to severe performance loss when performing prediction on real LR images, due to the inconsistency between the synthetic LR images and the physically captured LR images. Nevertheless, the deep learning approaches, thanks to their image-to-image transformation capability, can easily adapt. Instead of using the synthetic LR images, one can simply substitute them with the physical LR images, and doing so is not difficult as the

- *Y. Xie is with the Department of Computer Science and Engineering, Texas A&M University, College Station, TX 77843, USA, e-mail: (ethanyxc@tamu.edu).*
- *Y. Ding is with the Wm Michael Barnes'64 Department of Industrial and Systems Engineering, Texas A&M University, College Station, TX 77843, USA, e-mail: (yuding@tamu.edu).*
- *S. Ji is with the Department of Computer Science and Engineering, Texas A&M University, College Station, TX 77843, USA, e-mail: (sjj@tamu.edu).*

*Manuscript received xxx; revised xxx*

paired LR images are readily available.

While using the paired physical images takes care of, more or less, the aforementioned issues (a)–(c), [8] found that the performance of a deep learning approach depends heavily on how one actually uses the paired images for training. They investigated two strategies—one is known as the pooled-training, meaning that one mixes all training image-pairs in a common pool to train a single model, while the other strategy is self-training, which uses the HR/LR images from the same pair to train a specific model just for that pair. Naturally, with self-training, the number of the resulting models is the same as the number of image pairs. The pooled-training strategy is what has been commonly used in the deep learning super-resolution approaches, because this strategy provides far more image samples for training, which is, according to the conventional wisdom, a necessary factor ensuring the success of deep learning.

For the paired EM images, [8] instead found that using the self-training strategy produces more competitive results. Their reasoning is that for the paired images, as pointed in (d) above, there is a complete overlap, albeit a subset of the viewfield, between the LR and HR images. With this overlap, it is not surprising to see that the relationship learned directly from this specific pair is the best for boosting the resolution for the rest of the LR image area uncovered by the HR image. The numerical results presented by [8] support their claim rather convincingly—among seven methods tested, three of which are deep learning approaches, self-training outperforms pooled-training by a commanding margin for all of them.

While we acknowledge the existing deep learning methods may indeed be ill-equipped to take full advantage of pooled-training for the paired image case, staying with self-training has its own risk, due to two reasons: (i) The number of subimages produced by a single pair of images for training is rather limited. This limit in the amount of training images hampers the full potential of deep learning approaches, which are generally data hungry. (ii) Caring for and carrying around that many individual deep-learning models, each for a specific image pair, does not present itself as an enticing task, either.

In light of the potential shortcoming of self-training and the lack of capability of the current deep learning methods to effectively use pooled-training, the objective of this paper is therefore to devise a deep learning strategy that can make effective use of pooled-training and produce more competitive outcomes in paired EM image super-resolution than what is shown by [8].

Our specific strategy relies on the augmentation of the self-attention mechanism [9]. Firstly proposed in natural language processing, one approach to endow neural networks the capability to capture shared features among training instances is to augment the self-attention mechanism with learnable query [10]. [11] and [12] applied the attention mechanism with learnable query in the image domain, attempting to capture the inter-image dependencies and common features shared among images. However, to address the research question posed above for the paired EM image super-resolution, we found that the attention mechanism with learnable query does not produce the desired performance enhancement, due to the lacking of an

essential property in such mechanism, which is the spatially permutation equivariant required for image-to-image transformation tasks.

In this paper, we propose to augment the attention models with two components, the attention with shared references and the batch-aware attention in training. Based on the augmented attention model, we devise the Augmented Equivariant Attention Networks (AEANets), of which the attention block preserves the equivariance to any spatial permutations and thus makes the capturing of common features among images much more effective. We conduct experiments using the paired EM images made public by [8] to evaluate the performance and analyze the effectiveness of the proposed AEANets, in relative to other deep learning methods. Quantitative results show that our AEANets considerably outperforms the competitors, especially in terms of the clearness of the image and the quality of the foreground.

## 2 PRELIMINARIES AND RELATED STUDIES

In this section, we introduce the self-attention mechanism and related studies that apply the self-attention mechanism or its variations with learned query.

### 2.1 The Self-Attention Mechanism

The self-attention mechanism [9] has been widely applied to deep learning models in natural language processing (NLP) [13] and computer vision [14]. Compared to local operations such as convolutions that can only aggregate information locally, the self-attention mechanism is able to incorporate global information. Given an input feature map, the self-attention mechanism computes the relevance between every two locations on the feature map and aggregations information from one location to another according to the relevance. The self-attention mechanism hence endows neural networks the capability to capture long-range dependencies.

The self-attention mechanism can be applied to feature maps  $\mathcal{X} \in \mathbb{R}^{s_1 \times \dots \times s_k \times c}$  with any  $k \geq 1$  where  $k$  denotes the number of spatial dimensions,  $s_i$  denotes the spatial size along the  $i$ -th dimension and  $c$  denotes the number of features. For example, in a 2D image case, the self-attention mechanism is applied on the input  $\mathcal{X} \in \mathbb{R}^{w \times h \times c}$  where  $w$  and  $h$  denote the width and height of the image. Without loss of generality, we describe how the self-attention operator is performed in the 1D case ( $k = 1$ ), where there is only one spatial dimension. For higher-dimensional cases, the spatial dimensions can be unfolded into one dimension  $s = s_1 s_2 \dots s_k$  before being given to the self-attention operator. The output of the self-attention operator can then be folded back to the original shape as the final output.

In the 1D case, the self-attention operator takes as input a matrix  $\mathbf{X} \in \mathbb{R}^{s \times c}$  representing the features of a sequence, where  $s$  denotes its spatial dimension (*i.e.*, the length of the sequence or the spatial dimensions of unfolded images) and  $c$  denotes its feature dimension. The self-attention operator firstly computes three matrices, *i.e.*, the query  $\mathbf{Q}$ , the key  $\mathbf{K}$  and the value  $\mathbf{V}$ , by performing convolutions with kernel size of 1, to the input matrix  $\mathbf{X}$ . Formally,  $\mathbf{Q} = q(\mathbf{X}) \in \mathbb{R}^{s \times c_1}$ ,  $\mathbf{K} = k(\mathbf{X}) \in \mathbb{R}^{s \times c_1}$  and  $\mathbf{V} = v(\mathbf{X}) \in \mathbb{R}^{s \times c_2}$ , where

$q(\cdot), k(\cdot), v(\cdot)$  are three independent projections. Then, the output  $\mathbf{Y}$  of the attention operator is computed by

$$\mathbf{Y} = \text{Normalize}(\mathbf{Q} \cdot \mathbf{K}^T) \cdot \mathbf{V} \in \mathbb{R}^{s \times c_2}. \quad (1)$$

The function  $\text{Normalize}(\cdot)$  performs a normalization on the attention map  $\mathbf{Q} \cdot \mathbf{K}^T$  so that the values on the output  $\mathbf{Y}$  will not scale with the spatial size. Commonly used  $\text{Normalize}(\cdot)$  functions includes  $\text{Softmax}(\cdot)$  and the division by the spatial size of  $\mathbf{K}$ , *i.e.*,

$$\text{Normalize}(\mathbf{Q} \cdot \mathbf{K}^T) = \frac{1}{s}(\mathbf{Q} \cdot \mathbf{K}^T). \quad (2)$$

In this work, we use the normalization function in Equation (2). For clear comparisons, we use this type of normalization when describing all variations of the self-attention mechanisms in the rest of the paper.

Note that although the spatial sizes of  $\mathbf{Q}, \mathbf{K}, \mathbf{V}$  are the same in the self-attention mechanism, the spatial size  $s$  of the output is determined by the spatial size of query  $\mathbf{Q}$ . In addition, the feature size  $c_2$  of the output is determined by the feature size of value  $\mathbf{V}$ .

## 2.2 Attention Mechanism with Learned Query

A common variation of the attention mechanism is to directly learn the values in the query matrix  $\mathbf{Q}$ . In this case, the query  $\mathbf{Q}$  does not depend on the input  $\mathbf{X}$ . The attention mechanism with a learnable query is commonly used in NLP [10] and graph neural networks (GNNs) [15]. In certain domains such as biomedical image and nanoparticles, different images from one dataset usually share similar patterns and common features, such as microscopy images captured from different parts of tissue or tissues of the same type. The power of the learnable query has also been explored by previous studies in the biomedical image domain [12], [11]. In these cases, such a variation of the attention mechanism allows the networks to capture common features from all input images during training since the query is independent of the input and is shared by all input images.

Instead of computing the query from  $\mathbf{X}$ , the attention mechanism can learn a matrix  $\mathbf{Q} \in \mathbb{R}^{s_q \times c_1}$  independently of  $\mathbf{X}$ . The other computations in the attention mechanism with learnable query is then the same as the self-attention mechanism. Formally, with  $\mathbf{K} = K(\mathbf{X}) \in \mathbb{R}^{s \times c_1}$ ,  $\mathbf{V} = V(\mathbf{X}) \in \mathbb{R}^{s \times c_2}$  and a directly learned matrix  $\mathbf{Q} \in \mathbb{R}^{s_q \times c_1}$ ,

$$\mathbf{Y} = \text{Normalize}(\mathbf{Q} \cdot \mathbf{K}^T) \cdot \mathbf{V} \in \mathbb{R}^{s_q \times c_2}. \quad (3)$$

Since the spatial size of the output  $\mathbf{Y}$  is determined by the spatial size of  $\mathbf{Q}$ , the output size of the attention mechanism with learned query is no longer related to the spatial size of  $\mathbf{X}$ . As a result, when the attention mechanism with learned query is included in the neural network, the size of the output of the network is usually fixed.

## 3 MODEL AUGMENTATION WITH SHARED REFERENCES

Previous studies [12], [11] have explored different approaches to include a learnable query in the attention operator to capture common features among different images. Such attention operators with learnable query have been

shown to bring a promising performance boost, especially in NLP and image classification tasks. However, the attention operators with learnable query can, on the contrary, limit the performance of models for image-to-image transformation tasks such as image super-resolution, as such operators are not able to preserve an essential property required by the image-to-image transformation models, *i.e.*, the equivariance to spatial permutations.

In this section, we analyze the equivariance property in subsection 3.1, and show that such property is violated when the attention mechanism includes learned query in subsection 3.1. Based on our analysis, we propose in subsection 3.3 the attention operator with shared references that are able to capture common features among images without violating the equivariance property.

### 3.1 Equivariance and Invariance to Spatial Permutations

We introduce the equivariance property to spatial permutations by providing descriptions and formal definitions. We also introduce another related but different property, *i.e.*, the invariance to spatial permutations. We then show the importance of the equivariance property in image-to-image transformations. The spatial permutation includes a group of transformations to be applied to images. It is performed by permuting the spatial locations of any number of pixels or voxels in an image. Some common examples of spatial permutation include the rotation, the flipping and the shifting of an image. The equivariance to the spatial permutation is a property of an operator or a model such that applying a spatial permutation to the input of the operator or the model results in an equivalent effect of applying the same spatial permutation to the output. Taking the rotation as an example, when we rotate the input feature maps of an operator with such property by 90 degrees, its output will be correspondingly rotated by 90 degrees. On the contrary, if an operator is invariant to spatial permutations, then its output remains unchanged when permuting the input. We provide formal definitions of the spatial permutation, the equivariance and invariance property below.

**Definition 1.** Consider an image or feature map  $\mathbf{X} \in \mathbb{R}^{s \times c}$ , where  $s$  denotes the spatial dimension and  $c$  denotes the number of features. Let  $\pi$  denote a permutation of  $s$  elements. We call a transformation  $\mathcal{T}_\pi : \mathbb{R}^{s \times c} \rightarrow \mathbb{R}^{s \times c}$  a spatial permutation if  $\mathcal{T}_\pi(\mathbf{X}) = P_\pi \mathbf{X}$ , where  $P_\pi \in \mathbb{R}^{s \times s}$  denotes the permutation matrix associated with  $\pi$ , defined as  $P_\pi = [e_{\pi(1)}, e_{\pi(2)}, \dots, e_{\pi(s)}]^T$ , and  $e_i$  is a one-hot vector of length  $s$  with its  $i$ -th element being 1.

**Definition 2.** We call an operator  $A : \mathbb{R}^{s \times c_1} \rightarrow \mathbb{R}^{s \times c_2}$  to be spatially permutation equivariant if  $\mathcal{T}_\pi(A(\mathbf{X})) = A(\mathcal{T}_\pi(\mathbf{X}))$  for any  $\mathbf{X}$  and any spatial permutation  $\mathcal{T}_\pi$ . In addition, an operator  $A : \mathbb{R}^{s \times c_1} \rightarrow \mathbb{R}^{s \times c_2}$  is spatially permutation invariant if  $A(\mathcal{T}_\pi(\mathbf{X})) = A(\mathbf{X})$  for any  $\mathbf{X}$  and any spatial permutation  $\mathcal{T}_\pi$ .

We now compare the two properties. We argue that while the image classification models could benefit from the invariance to spatial permutations according to previous studies [16], [17], an image-to-image transformation model requires the equivariance to spatial permutations.

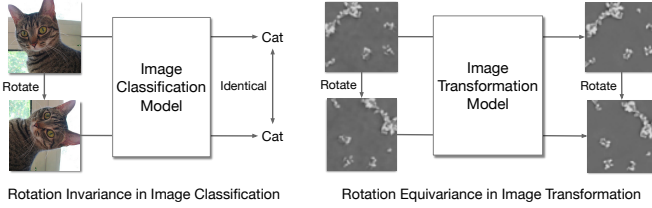


Fig. 1. Examples that compare the invariance property with the equivariance property. Tasks such as classification require spatial permutation (e.g., rotation) invariant models, where applying the permutation to the input does not change the output of the model. On the contrary, the image transformation tasks require spatial permutation (e.g., rotation) equivariant models, where applying the permutation to the input leads to the same permutation applied to the output of the model.

We consider the properties under three common spatial permutation cases, *i.e.*, rotation, flipping and shifting.

In a natural image classification task, when the input image is rotated, flipped or shifted, we expect the classification result to remain the same as long as the object to be classified is still in the image, as shown in Figure 1 (left). In this case, the model can benefit from its invariance property and an operator that is spatial permutation invariant can help the model realize such property and hence improve its generalization capability.

However, when performing the rotation, flipping or shifting on the input of an image-to-image transformation model, we expect the output image of the model to be rotated, flipped or shifted correspondingly, as shown in Figure 1 (right). Hence the equivariance to spatial permutation is desired by the model. In this case, if a spatial permutation invariant operator is included, the equivariance will be violated, since the operator outputs a constant tensor while the input image is rotated, flipped or shifted. Hence, operators with such an invariant property can be inappropriate in image-to-image transformation models and may lead to a performance reduction. It is desirable to use a spatial permutation equivariant operator to preserve the equivariance of the model.

### 3.2 Spatial Permutation Properties of Attention Operators

We now analyze the properties of the two types of attention operators regarding the spatial permutation using the same notations as in Section 2.1 and Section 2.2. Intuitively, when a spatial permutation is performed on the input of an attention operator, the corresponding permutation made on the key  $\mathbf{K}$  and the value  $\mathbf{V}$  does not result in any difference in the output, as long as the same permutation is applied to both  $\mathbf{K}$  and  $\mathbf{V}$ . In fact, the order of spatial locations on the output feature map is determined by the spatial locations on the query  $\mathbf{Q}$ . Hence the attention operator is permutation equivariant as long as  $\mathbf{Q}$  is obtained from  $\mathbf{X}$ .

For simplicity, we denote  $A_s$  a self-attention operator and  $A_Q$  an attention operator with learned query. The outputs  $\mathbf{Y}$  of the two operators are therefore equal to  $A_s(\mathbf{X})$  and  $A_Q(\mathbf{X})$ . We show that the following theorem holds.

**Theorem 1.** *A self-attention operator  $A_s$  is permutation equivariant while an attention operator with learned query  $A_Q$  is*

*permutation invariant. In particular, letting  $\mathbf{X}$  denote the input matrix and  $\mathcal{T}$  denotes any spatial permutation, we have*

$$A_s(\mathcal{T}_\pi(\mathbf{X})) = \mathcal{T}_\pi(A_s(\mathbf{X})),$$

and

$$A_Q(\mathcal{T}_\pi(\mathbf{X})) = A_Q(\mathbf{X}).$$

*Proof.* When applying a spatial permutation  $\mathcal{T}_\pi$  to the input  $\mathbf{X}$  of a self-attention operator  $A_s$ , we have

$$\begin{aligned} A_s(\mathcal{T}_\pi(\mathbf{X})) &= \left( \frac{1}{s} \mathcal{T}_\pi(\mathbf{Q}) \cdot (\mathcal{T}_\pi(\mathbf{K}))^T \right) \cdot \mathcal{T}_\pi(\mathbf{V}) \\ &= \frac{1}{s} P_\pi \mathbf{Q} \mathbf{K}^T (P_\pi^T P_\pi) \mathbf{V} \\ &= P_\pi \left( \frac{1}{s} \mathbf{Q} \mathbf{K}^T \right) \mathbf{V} \\ &= \mathcal{T}_\pi(A_s(\mathbf{X})). \end{aligned} \quad (4)$$

Note that  $P_\pi^T P_\pi = I$  since  $P_\pi$  is an orthogonal matrix. Since convolutions with a kernel size of 1 are permutation equivariant, the projected  $\mathbf{Q} = q(\mathbf{X})$ ,  $\mathbf{K} = k(\mathbf{X})$ ,  $\mathbf{V} = v(\mathbf{X})$  are spatial permutation equivariant with respect to the input  $\mathbf{X}$ . By showing  $A_s(\mathcal{T}_\pi(\mathbf{X})) = \mathcal{T}_\pi(A_s(\mathbf{X}))$  we have shown that  $A_s$  is spatial permutation equivariant according to Definition 2.

In comparison, when applying  $\mathcal{T}_\pi$  to the input of an attention operator  $A_Q$  with a learned query  $\mathbf{Q}$ , which is independent of the input  $\mathbf{X}$ , we have

$$\begin{aligned} A_Q(\mathcal{T}_\pi(\mathbf{X})) &= \left( \frac{1}{s} \mathbf{Q} \cdot (\mathcal{T}_\pi(\mathbf{K}))^T \right) \cdot \mathcal{T}_\pi(\mathbf{V}) \\ &= \frac{1}{s} \mathbf{Q} \mathbf{K}^T (P_\pi^T P_\pi) \mathbf{V} \\ &= \left( \frac{1}{s} \mathbf{Q} \mathbf{K}^T \right) \mathbf{V} \\ &= A_Q(\mathbf{X}). \end{aligned} \quad (5)$$

Since  $A_Q(\mathcal{T}_\pi(\mathbf{X})) = A_Q(\mathbf{X})$ , we have shown that  $A_Q$  is spatial permutation invariant according to Definition 2.  $\square$

Note that the above theorem still holds when the Softmax is applied for normalization, the proof of which can be found in [18].

### 3.3 Augmented Attention with Shared References

We have shown that an image-to-image transformation model requires equivariance to spatial permutations while the attention operator with learned query is permutation invariant. Although the attention operator with learned query endows models the capability to capture common features among images, the invariance property makes it inappropriate to be applied in image-to-image transformation tasks. In order to endow the attention operator the capability to capture common features among images without losing the equivariance property, we propose an attention operator augmented with learnable shared references, as opposed to shared query. The shared references are represented by a matrix consisting of learnable variables and are augmented to the key and value matrices along the spatial dimensions.

To be concrete, given the flattened input feature map  $\mathbf{X} \in \mathbb{R}^{wh \times c}$  where the width  $w$  and height  $h$  are flattened into one dimension and  $c$  is the number of features, the

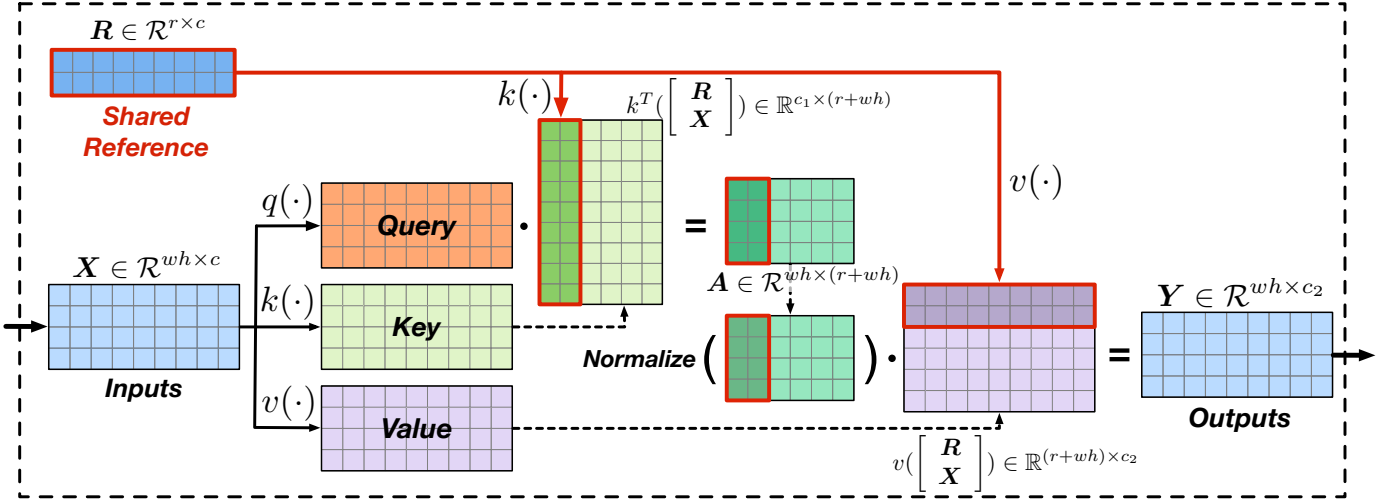


Fig. 2. Comparison between the original self-attention (top) and proposed attention operator with shared references (bottom). Given the flattened input matrix  $X$  of shape [width  $\times$  height, channels], the proposed attention operator train a reference matrix of shape [reference size, channels], which is used to compute the key and value. The highlighted parts in the key and value are related to the shared references and the rest parts are related to the input image. The spatial size of the output is the same as the spatial size of the query.

shared references are represented by a learnable matrix  $R \in \mathbb{R}^{r \times c}$ , where  $r$  is the size of the shared references as a hyper-parameter. The learned shared references is projected by  $k(\cdot)$  and  $v(\cdot)$  into the same space of key and value. The computation of an attention operator augmented with shared references  $A_R$  can be formally expressed as

$$\tilde{X} = \begin{bmatrix} R \\ X \end{bmatrix} \in \mathbb{R}^{(r+wh) \times c}, \quad (6)$$

$$A_R(X) = \frac{1}{r+wh} (q(X) \cdot k^T(\tilde{X})) \cdot v(\tilde{X}),$$

where  $k^T(\tilde{X})$  denotes the transposed key  $k(\tilde{X})$ . Note that the key  $\tilde{K} = k(\tilde{X})$  and value  $\tilde{V} = v(\tilde{X})$  are computed from  $\tilde{X}$ , while the query  $Q$  is computed from  $X$ . The operator with shared references is illustrated in Figure 2. We now show the property of the proposed attention operator  $A_R$  in the following theorem.

**Theorem 2.** *The proposed augmented attention operator with shared references  $A_R$  is spatially permutation equivariant, i.e.,*

$$A_R(\mathcal{T}_\pi(X)) = \mathcal{T}_\pi(A_R(X)).$$

*Proof.* We let  $\tilde{P}_\pi = \begin{pmatrix} I_r & 0 \\ 0 & P_\pi \end{pmatrix}$ , where  $P_\pi$  is the permutation matrix applied to  $X$ . Then we have

$$\begin{aligned} A_R(\mathcal{T}_\pi(X)) &= \left( \frac{1}{r+wh} \mathcal{T}_\pi(Q) \cdot (\tilde{P}_\pi \tilde{K})^T \right) \cdot \tilde{P}_\pi \tilde{V} \\ &= \frac{1}{r+wh} P_\pi Q \tilde{K}^T (\tilde{P}_\pi^T \tilde{P}_\pi) \tilde{V} \\ &= P_\pi \left( \frac{1}{r+wh} Q \tilde{K}^T \right) \tilde{V} \\ &= \mathcal{T}_\pi(A_R(X)). \end{aligned} \quad (7)$$

This shows that the proposed attention operator augmented with shared references is spatially permutation equivariant.  $\square$

Compared with the original self-attention operators in which the key and value matrices are fully based on the input, the key and value of  $A_R$  contain additional information about the features shared by all images in the dataset. The learning process of the shared reference is to distill common features from images in the entire training data. Each spatial location on an input instance aggregates information not only globally from the input instance itself, but also from the distilled references shared by all the input images.

#### 4 MODEL AUGMENTATION WITH BATCH-AWARE TRAINING

A common strategy to train a deep model is to feed a mini-batch of images to the network at each training step. The mini-batch is referred to as batch in the following paragraphs for short. When a self-attention operator is included, the operator processes the batch at an instance level. Given an input batch of feature maps  $\{X_1, \dots, X_N\}$ , where  $N$  is the batch size, the self-attention operator computes the outputs individually for each instance in the batch, i.e.,  $Y_i = A_s(X_i)$  for  $i = 1, \dots, N$ .

In the case where images in a dataset share similar patterns, the performance of a deep model can further benefit by incorporating cross-images dependencies. In this case, the learning of such dependencies across images in a batch can be of great importance. Due to the non-local property, the attention operators can be extended from the instance level to a batch level in order to learn the correlations across images in a batch. Formally, we define an augmented batch-aware operator  $A_{batch}$  such that

$$Y_i = A_{batch}(X_i; X_1, \dots, X_N), i = 1, \dots, N.$$

In this case, the computation of each output instance is aware of the other instances in the current batch. In order to realize such an augmentation, we propose a training

strategy with this batch-aware attention, where the key and value cover all the images in the training batch. That is,

$$A_{batch}(\mathbf{X}_i; \mathbf{X}_1, \dots, \mathbf{X}_N) = \frac{1}{Nwh} q(\mathbf{X}_i) \cdot k^T \left( \begin{bmatrix} \mathbf{X}_1 \\ \vdots \\ \mathbf{X}_N \end{bmatrix} \right) \cdot v \left( \begin{bmatrix} \mathbf{X}_1 \\ \vdots \\ \mathbf{X}_N \end{bmatrix} \right), \quad (8)$$

where  $k(\cdot)$  and  $v(\cdot)$  are the projections defined in the original self-attention.

The proposed batch-aware attention aggregates information from the entire batch based on the correlation across images for each input location. Since each batch is uniformly sampled from the entire dataset, the aggregation from batches can estimate the information aggregation from the entire dataset. The weights of the projections  $q(\cdot)$ ,  $k(\cdot)$ ,  $v(\cdot)$  in batch-aware attention and the attention with shared references are shared during training. The purpose of including the batch-aware attention in training is to help the distill of shared references and learn better projections in attention by using cross-image dependencies. In our experiments, we empirically show that additional performance improvements can be achieved by including the augmented batch-aware attention in training.

## 5 AUGMENTED EQUIVARIANT ATTENTION NETWORKS

### 5.1 The Augmented Equivariant Attention Block

The proposed augmented equivariant attention block consists of a branch for the attention operator  $A_R$  with shared references and a branch for the batch-aware attention  $A_{batch}$ . In the attention block, the weights in each projection of  $q(\cdot)$ ,  $k(\cdot)$  and  $v(\cdot)$  are shared by the two attention operators  $A_R$  and  $A_{batch}$ . As the attention block performs differently during training and prediction, we individually describe how it works during training and prediction.

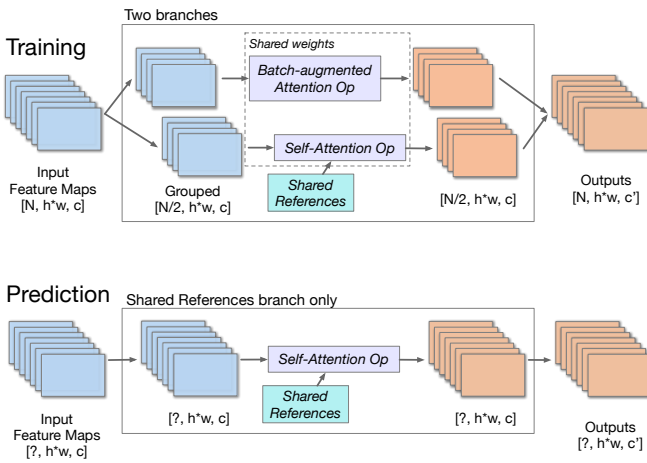


Fig. 3. The proposed attention block. During training (top), both branches are used. The input batch are splitted into two groups and passed to the two operators. The outputs of the two operators are then merged together. For prediction (bottom), only the branch with shared references is used.

During training, both the  $A_R$  and  $A_{batch}$  are used. Given an input batch  $\{\mathbf{X}_1, \dots, \mathbf{X}_N\}$  to the block, the

batch is evenly split into two groups  $\{\mathbf{X}_1, \dots, \mathbf{X}_{\lfloor N/2 \rfloor}\}$  and  $\{\mathbf{X}_{\lfloor N/2 \rfloor + 1}, \dots, \mathbf{X}_N\}$  as the inputs to the two branches. The outputs of the two branches are then merged back into a complete batch. While the batched data in the two branches are separate, the parameters of the two branches are shared.

Once the network is trained, the parameters in the two operators are fixed and are used by the attention operation with shared references during prediction. The batch-aware attention is excluded during prediction since there is not necessarily a batch input during prediction. In other words, the branch that contains the batch-aware attention operator is disabled, and all input data flow into the  $A_R$  branch. In spite of the exclusion of the batch-aware attention, the existence of shared references distilled from training images allows the model to still utilize the dependencies between training images and the given input image for prediction. Figure 3 illustrates how the block works during training and prediction.

### 5.2 Network Architecture

Recent studies have shown that the U-Net [19] architecture achieves promising performance in many image transformation tasks, especially for microscopy images [11], [20], [21]. In this work, we use the U-Net as the base network architecture of our model. To be specific, we use a U-Net with a depth of 3 (including two down-sampling operations and up-sampling operations, respectively). The skip-connections in the U-Net are merged into the up-sampling path by concatenation.

To enable the use of the proposed augmented attention within the U-Net architecture, we follow [22] to (1) include a residual connection in the attention block by addition and (2) substitute the bottom block in the original U-Net with our proposed attention block. The overall architecture of the proposed network is shown in Figure 4.

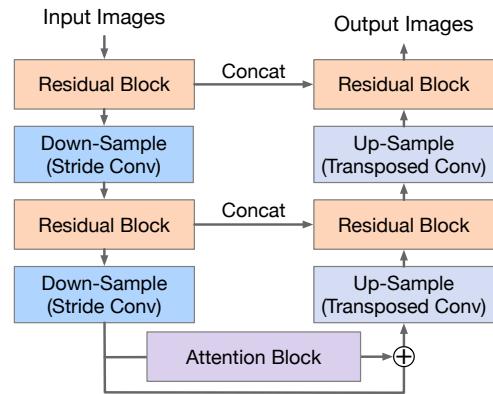


Fig. 4. Network Architecture. We chip our proposed attention block into a U-Net architecture with depth of 3. The skip-connections in the U-Net use concatenation. The down-sampling and up-sampling apply the stride convolution and transposed convolution respectively.

Note that although we use the augmented attention block as the bottom block in the U-Net architecture, it can be inserted into any other deep architectures, thereby capturing non-local and cross-image dependencies and the common features shared by the entire dataset.

## 6 EXPERIMENTAL RESULTS

### 6.1 Dataset and Experimental Setup

#### 6.1.1 The Paired EM Image Dataset

In this experimental study, we use the paired EM images dataset used in [8] to train and evaluate our model.<sup>1</sup> To recap, the paired image dataset consists of 22 pairs of LR and HR nanoimages of size  $1,280 \times 944$ . The LR and HR nanoimages are captured by the same scanning electron microscope (SEM) at two different magnifications. Specially, the HR image is two times zoomed-in from the LR image and the field of view (FOV) of the HR image is covered by the FOV of the LR image, *i.e.*, the HR image corresponds to a  $1/4$  sub-area of the LR image.

#### 6.1.2 Image-Pairs Preprocessing

We perform several preprocessing on the original LR and HR images to build our dataset for training and testing. We first perform the Random Sample Consensus [23] (RANSAC) algorithm to register the HR images in the corresponding areas in the LR images, based on the ORB features [24]. We select the registered area in each LR image and use a bicubic interpolation to upsample the selected LR subareas to be of the same size of the HR images, *i.e.*,  $1,280 \times 944$ . Through the preprocessing, the resulting LR and HR images refer to the same area but are in different resolutions.

#### 6.1.3 Training-Test Split and Training Strategies

We follow [8] for creating the training-test split. In particular, the area of each image is divided into  $3 \times 4$  subimages. Among the 12 patches, the left-sided  $3 \times 3$  area is used for training and the right-sided  $1 \times 3$  area is used for testing. During testing, the evaluation metrics are computed on the testing patches individually and then averaged. Figure 5 in [8] presents a graphic illustration of the training-test split.

As mentioned in Section 1, [8] studied two training strategies: self-training and pooled-training. We evaluate our methods under the same two training strategies. The pooled-training trains a single model on all the 22 image pairs. With the splitting of the original images into  $3 \times 4$  smaller subimages, in the pooled-training, the 22 image pairs become a total of 198 subimage pairs for training and 66 subimage pairs for test. The evaluation metrics are computed on each testing subimage and then averaged. The self-training trains one model for each of the 22 image pairs and results in a total of 22 models. For each model, the training pair is 9 and the test pair is 3. The overall performance is to average the metrics across all image pairs.

### 6.2 Evaluation Results

We follow [8] and use the Paired EM Image Dataset for evaluation. The detailed dataset description and experimental setup is provided in Appendix 4. We evaluate our method and compare it with an array of deep learning-based baselines. In addition to three deep learning methods compared in [8], *i.e.*, VDSR [25], RCAN [26], and EDSR [27],

we further include the original U-Net [19] and GVTNets [22] in this comparison study. The U-Net, GVTNets, and our proposed AEANets use the same network architecture setting except for the attention blocks. We also include the SOTA non-deep-learning-based method, which is the paired LB-NLM [8] in our baselines. We use two evaluation metrics, the structural similarity index measure (SSIM) and peak signal-to-noise ratio (PSNR), calculated between the prediction and the corresponding HR images (ground truth). We show in Table 1 the averaged improvements in terms of the two metrics, as compared to the input LR image (*i.e.*, after bicubic interpolation). The improvement is denoted as  $\Delta$ PSNR and  $\Delta$ SSIM.

The results show that the AEANets model with pooled-training significantly outperforms the baselines with the same training strategy. More importantly, the performance of AEANets with pooled-training is better than the baseline models with self-training, indicating that the self-training is no longer required for our proposed AEANets. In other words, AEANets can be used more efficiently, leading to better performance, and can be applied in broader scenarios where self-training may not be applicable.

While the improvement in terms of PSNR is moderate, the improvement in terms of SSIM is much more remarkable, a 70% increase as compared to the best of the three deep learning methods originally used in [8]. Recall that SSIM measures how far away an image is from the HR image and a higher SSIM suggests a better capability of the resulting image to show finer details. The improvement in SSIM bears important practical implication for material characterization.

To see the implication from a different angle, consider the image quality improvement only in the foreground of the images. Not surprisingly, material scientists are more interested in the nanomaterial clusters (foreground) than the host material (background) in their applications. To separate the foreground and background, we follow [8] and perform Otsu’s algorithm on each testing patch. We compute the improvements in PSNR on the foreground and background for the following methods: VDSR, SRSW, Paired LB-NLM and AEANets. The outcome is shown in Table 1 (right). The results demonstrate that although VDSR with self-training achieves a higher PSNR in the background, AEANets outperform the three aforementioned methods for the foreground. This outcome reinforces the advantage of AEANets shown in the SSIM comparison.

In terms of the foreground-background difference, [8] in fact commented that “*It is apparent that all these methods [those included in their paper] denoise the background much more than they enhance the foreground.*” While AEANets still see a greater PSNR improvement over its background, its foreground-background performance gap is the smallest among the four alternatives in Table 1 (right). The practical implication is that AEANets are a better tool for material characterization.

We also include some visualization results for compare the super-resolution performance of AEANets with that of U-Net. The visualization shows that the predictions from AEANets have clearer edges of the nanomaterial clusters. It is also worth mentioning that the deep learning-based methods, including U-Net and AEANets, have an additional

<sup>1</sup> The paired EM images dataset is available for public access at <https://aml.engr.tamu.edu/2001/09/01/publications/> (then go to J74).

TABLE 1

*Left:* Comparison of performance quantified by image quality improvement in terms of PSNR and SSIM, among our methods and the baseline models. Bold numbers are the highest compared among results in both training strategies. *Right:* Improvements in PSNR on foreground (nanomaterial clusters) and background (host material) individually. “Self” in the brackets after method names refers to self-training.

Methods	Pooled-training		Self-training		Methods	Foreground	Background
	$\Delta$ PSNR (dB)	$\Delta$ SSIM	$\Delta$ PSNR (dB)	$\Delta$ SSIM			
VDSR [25]	1.25	0.047	2.07	0.051	VDSR (Self)	0.97	<b>2.83</b>
RCAN [26]	1.59	0.051	2.07	0.050	SRSW (Self)	-0.25	2.15
EDSR [27]	1.35	0.051	2.06	0.052	Paired LB-NLM (Self)	0.23	2.65
Paired LB-NLM [8]	0.78	0.031	1.67	0.037	AEANet	<b>1.15</b>	2.42
U-Net [19]	1.46	0.074	1.42	0.036			
GVTNet [22]	1.87	0.086	1.81	0.078			
AEANet (Ours)	<b>2.10</b>	<b>0.087</b>	1.06	0.032			

denoising effect in the background. We believe that the effect is due to the noise in the LR image and HR image belongs to the same noise distribution but are independently sampled, which satisfies the requirements of the Noise2Noise [28] denoising. The denoising effect could be less likely to occur in synthetic super-resolution datasets. Compared to U-Net, AEANets can perform better denoising, as shown in Figure 5.

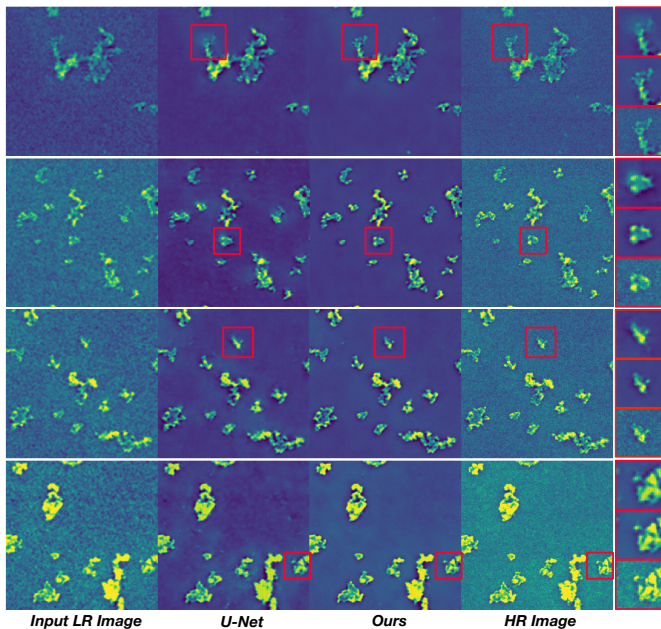


Fig. 5. Visualization of the output of super-resolution models on four testing patches. From left to right, the columns are input LR images, outputs of the U-Net, outputs of our model and the ground truth HR images). We select some areas to zoom in for a better view. From top to bottom, smaller patches on the right are zoomed-in from U-Net, our model and the HR images.

### 6.3 Effects of Shared References

This subsection provides a discussion on the effects of shared references. Recall that in the learned shared references  $\mathbf{R} = [\mathbf{f}_1, \dots, \mathbf{f}_r]^T \in \mathbb{R}^{r \times c}$  of size  $r$ , we call each row vector  $\mathbf{f}_i \in \mathbb{R}^{1 \times c}$  the feature vector of an abstract pixel distilled from the training images. To illustrate the effects of the shared references, we select three input images and randomly select the feature vectors of four abstract pixels. We visualize how much the Query matrix  $\mathbf{Q}$  of the three images is correlated

to the four abstract pixels. Provided the Query matrix  $\mathbf{Q}_i \in \mathbb{R}^{wh \times c_1}$  of an input image and the feature vector  $\mathbf{f}_j$  of an abstract pixel, we visualize

$$\mathbf{Q}_i \cdot \mathbf{k}^T(\mathbf{f}_j) \in \mathbb{R}^{wh \times 1}, i \in \{1, 2, 3\}, j \in \{1, 2, 3, 4\},$$

where  $\mathbf{k}(\cdot)$  projects the feature vector into the Key space and the dot product indicates the relevance between each pixel in the input image and the learned abstract pixel. We fold  $\mathbf{Q}_i \cdot \mathbf{k}^T(\mathbf{f}_j)$  back to the original 2D spatial shape  $w \times h$  and visualize it in Figure 6 for each  $(i, j)$  in the form of a heatmap. The visualization shows which pixels (or segments) in the input image are tightly related to a given abstract pixel in the shared references.

The four columns on the right show different patterns, suggesting that the abstract pixels in the shared references contain different types of features and are related to different segments of the input images. The abstract pixels in the same column show similar patterns, indicating that features captured by the abstract pixels are shared across images. These two observations tell us that the effect of the shared references matches our expectation.

### 6.4 Ablation Studies

We conduct an ablation study to analyze (1) how the shared references and the Batch-aware Attention mechanism help improve the performance of attention-based models and (2) how AEANets benefit from a larger input image size. For a fair comparison, all the models in this subsection are trained with pooled-training.

We first evaluate the performance of AEANets with the following options: Batch-aware Attention excluded, shared references excluded, and shared references with different sizes (16, 32 and 64). The results in terms of  $\Delta$ PSNR and  $\Delta$ SSIM are shown in Table 2. Compared to the original attention-based model, GVTNets, applying Batch-aware Attention and shared references renders a performance gain of 0.09 dB and 0.17 dB, respectively. When increasing the size of the shared references, the performance of AEANets also increases.

Regarding the size of input images, we evaluate AEANets on the same testing images but with different input sizes. In particular, we crop each image into patches of a given size, input the patches to the network and then stitch the predicted patches together as the prediction of the entire image. We evaluate the improvement in PSNR for each size and show the results in Figure 7. Among the

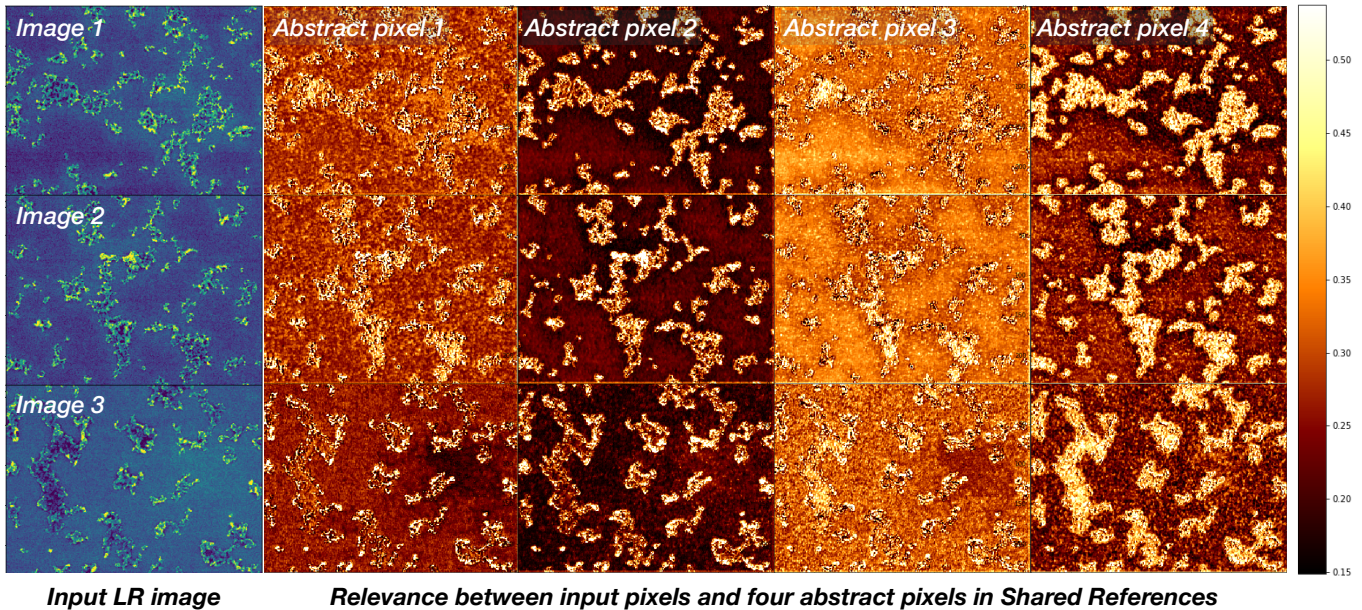


Fig. 6. The visualization of the relevance between pixels in the input image and four randomly selected abstract pixels from shared references. From top to bottom, rows are the visualizations of different input images. From left to right, the first column shows the input images and the rest four columns are the visualizations for the four selected abstract pixels. A higher value in the heatmap indicates stronger relevance.

TABLE 2

Performance of AEANets when Batch-aware Attention is excluded or the size of shared references are decreased. Three baseline methods are also given for comparison.

Methods	$\Delta$ PSNR (dB)	$\Delta$ SSIM
RCAN	1.59	0.051
U-Net	1.46	0.074
GVTNets	1.87	0.086
Shared Reference (SR) only	2.04	0.085
Batch-Aware (BA) only	1.96	0.084
BA + SR (16)	1.98	0.085
BA + SR (32)	2.02	0.085
BA + SR (64)	<b>2.10</b>	<b>0.087</b>

evaluated alternative, both GVTNet and AEANets benefit from a larger patch size since both are attention-based models. It is interesting to see that the performance of GVTNet with full-sized input can be achieved by AEANets with much smaller input patch sizes. Specifically, the AEANet with shared references of size 64 and the input size 256 reaches the similar performance of the GVTNet with full-sized input.

## 7 CONCLUSION

High-resolution EM images are usually desired for better Biomedical and Nanomaterial researches. Computational methods that perform super-resolution on low-resolution EM images make it possible to obtain high-resolution EM images more efficiently with lower cost. In this work, we consider the super-resolution as an image-to-image transformation and focus on challenges in the case where both high-resolution and low-resolution images in the training dataset are physically captured. To address the challenges, we have introduced the Augmented Equivariant Attention Networks (AEANets), which is able to utilize shared features among

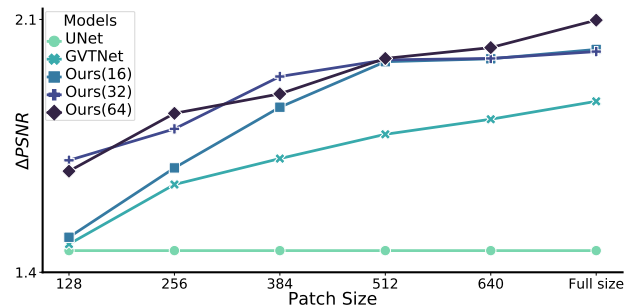


Fig. 7. The output image quality  $\Delta$ PSNR over different input patch sizes. Results are computed on testing images. Numbers inside the brackets in models, *i.e.*, 16, 32 and 64, refer to the sizes of shared references for our methods. For all attention-based methods (GVTNet and ours), the output image quality increases when larger input patches are given.

images and inter-image dependencies, and preserve the spatially permutation equivariant property for image-to-image transformation. We have theoretically analysed the property of the proposed attention operator augmented by shared references and the property of existing attention operators as comparisons. In addition, we have conducted experiments to show the effectiveness of AEANets.

## ACKNOWLEDGEMENTS

The authors would like to acknowledge the generous support from their sponsors. This work is partially supported by AFOSR DDIP program grant FA9550-18-1-0144, NSF grants IIS-1849085 and DBI-2028361, and Texas A&M X-grant program.

## REFERENCES

- [1] R. Y. Tsai and T. S. Huang, "Multiframe image restoration and registration," in *Advances in Computer Vision and Image Processing*, T. S. Huang, Ed. Greenwich, CT: JAI Press Inc., 1984, vol. 1, pp. 317–339.

- [2] W. T. Freeman, E. C. Pasztor, and O. T. Carmichael, "Learning low-level vision," *International Journal of Computer Vision*, vol. 40, no. 1, pp. 25–47, 2000.
- [3] W. T. Freeman, T. R. Jones, and E. C. Pasztor, "Example-based super-resolution," *IEEE Computer Graphics and Applications*, vol. 22, no. 2, pp. 56–65, 2002.
- [4] C. Dong, C. C. Loy, K. He, and X. Tang, "Image super-resolution using deep convolutional networks," *IEEE Transactions on Pattern Analysis and Machine Intelligence*, vol. 38, no. 2, pp. 295–307, 2016.
- [5] M. Weigert, U. Schmidt, T. Boothe, A. Müller, A. Dibrov, A. Jain, B. Wilhelm, D. Schmidt, C. Broaddus, S. Culley, M. Rocha-Martins, F. Segovia-Miranda, C. Norden, R. Henriques, M. Zerial, M. Solimena, J. Rink, P. Tomancak, L. Royer, F. Jug, and E. W. Myers, "Content-aware image restoration: pushing the limits of fluorescence microscopy," *Nature Methods*, vol. 15, no. 12, pp. 1090–1097, 2018.
- [6] E. Nehme, L. E. Weiss, T. Michaeli, and Y. Shechtman, "Deep-storm: super-resolution single-molecule microscopy by deep learning," *Optica*, vol. 5, no. 4, pp. 458–464, 2018.
- [7] Z. Luo, A. Yurt, R. Stahl, A. Lambrechts, V. Reumers, D. Braeken, and L. Lagae, "Pixel super-resolution for lens-free holographic microscopy using deep learning neural networks," *Optics Express*, vol. 27, no. 10, pp. 13 581–13 595, 2019.
- [8] Y. Qian, J. Xu, L. F. Drummy, and Y. Ding, "Effective super-resolution methods for paired electron microscopic images," *IEEE Transactions on Image Processing*, vol. 29, pp. 7317–7330, 2020.
- [9] A. Vaswani, N. Shazeer, N. Parmar, J. Uszkoreit, L. Jones, A. N. Gomez, Ł. Kaiser, and I. Polosukhin, "Attention is all you need," in *Proceedings of the 31st International Conference on Neural Information Processing Systems*, 2017, pp. 5998–6008.
- [10] Z. Yang, D. Yang, C. Dyer, X. He, A. Smola, and E. Hovy, "Hierarchical attention networks for document classification," in *Proceedings of the 2016 Conference of the North American chapter of the Association for Computational Linguistics: Human Language Technologies*, 2016, pp. 1480–1489.
- [11] Y. Liu, H. Yuan, Z. Wang, and S. Ji, "Global pixel transformers for virtual staining of microscopy images," *IEEE Transactions on Medical Imaging*, vol. 39, no. 6, pp. 2256–2266, 2020.
- [12] H. Yuan, N. Zou, S. Zhang, H. Peng, and S. Ji, "Learning hierarchical and shared features for improving 3d neuron reconstruction," in *Proceedings of the 19th IEEE International Conference on Data Mining*. IEEE, 2019, pp. 806–815.
- [13] J. Devlin, M.-W. Chang, K. Lee, and K. Toutanova, "BERT: Pre-training of deep bidirectional transformers for language understanding," in *Proceedings of the 2019 Conference of the North American Chapter of the Association for Computational Linguistics: Human Language Technologies, Volume 1 (Long and Short Papers)*. Minneapolis, Minnesota: Association for Computational Linguistics, Jun. 2019, pp. 4171–4186. [Online]. Available: <https://www.aclweb.org/anthology/N19-1423>
- [14] X. Wang, R. Girshick, A. Gupta, and K. He, "Non-local neural networks," in *Proceedings of the IEEE Conference on Computer Vision and Pattern Recognition*, 2018, pp. 7794–7803.
- [15] Y. Li, D. Tarlow, M. Brockschmidt, and R. S. Zemel, "Gated graph sequence neural networks," in *4th International Conference on Learning Representations*, Y. Bengio and Y. LeCun, Eds., 2016.
- [16] D. Marcos, M. Volpi, and D. Tuia, "Learning rotation invariant convolutional filters for texture classification," in *Proceedings of the 23rd International Conference on Pattern Recognition*. IEEE, 2016, pp. 2012–2017.
- [17] R. Zhang, "Making convolutional networks shift-invariant again," in *Proceedings of the 36th International Conference on Machine Learning*, 2019.
- [18] S. Ji, Y. Xie, and H. Gao, "A mathematical view of attention models in deep learning," Texas A&M University, April 2019. [Online]. Available: <http://people.tamu.edu/~sji/classes/attn.pdf>
- [19] O. Ronneberger, P. Fischer, and T. Brox, "U-net: convolutional networks for biomedical image segmentation," in *Proceedings of the 18th International Conference on Medical Image Computing and Computer-assisted Intervention*. Springer, 2015, pp. 234–241.
- [20] Z. Wang, N. Zou, D. Shen, and S. Ji, "Non-local U-nets for biomedical image segmentation," in *Proceedings of the 34th AAAI Conference on Artificial Intelligence*, 2020, pp. 6315–6322.
- [21] T. Zeng, B. Wu, and S. Ji, "DeepEM3D: Approaching human-level performance on 3D anisotropic EM image segmentation," *Bioinformatics*, vol. 33, no. 16, pp. 2555–2562, 2017.
- [22] Z. Wang, Y. Xie, and S. Ji, "Global voxel transformer networks for augmented microscopy," *arXiv preprint arXiv:2008.02340*, 2020.
- [23] M. A. Fischler and R. C. Bolles, "Random sample consensus: a paradigm for model fitting with applications to image analysis and automated cartography," *Communications of the ACM*, vol. 24, no. 6, pp. 381–395, 1981.
- [24] E. Rublee, V. Rabaud, K. Konolige, and G. Bradski, "Orb: an efficient alternative to sift or surf," in *Proceedings of the 2011 International Conference on Computer Vision*. IEEE, 2011, pp. 2564–2571.
- [25] J. Kim, J. Kwon Lee, and K. Mu Lee, "Accurate image super-resolution using very deep convolutional networks," in *Proceedings of the IEEE Conference on Computer Vision and Pattern Recognition*, 2016, pp. 1646–1654.
- [26] Y. Zhang, K. Li, K. Li, L. Wang, B. Zhong, and Y. Fu, "Image super-resolution using very deep residual channel attention networks," in *Proceedings of the European Conference on Computer Vision*, 2018, pp. 286–301.
- [27] B. Lim, S. Son, H. Kim, S. Nah, and K. Mu Lee, "Enhanced deep residual networks for single image super-resolution," in *Proceedings of the IEEE Conference on Computer Vision and Pattern Recognition Workshops*, 2017, pp. 136–144.
- [28] J. Lehtinen, J. Munkberg, J. Hasselgren, S. Laine, T. Karras, M. Aittala, and T. Aila, "Noise2noise: Learning image restoration without clean data," in *Proceedings of the 35th International Conference on Machine Learning*, vol. 80, 2018, pp. 2971–2980.